852. Study of characteristic variations of high-speed spindles induced by centrifugal expansion deformations

Hongrui Cao[1], Tomas Holkup[2], Xuefeng Chen[3], Zhengjia He[4]
[1, 3, 4] State Key Laboratory for Manufacturing Systems Engineering, Xi'an Jiaotong University
Xi'an 710049, P. R. China
[2]Research Center of Manufacturing Technology, Czech Technical University in Prague, Czech Republic
E-mail: [1]*chr@mail.xjtu.edu.cn*, [2]*T.Holkup@rcmt.cvut.cz*, [3]*chenxf@mail.xjtu.edu.cn*, [4]*hzj@mail.xjtu.edu.cn*
(Received 1 June 2012; accepted 4 September 2012)

Abstract. High-speed machining has continuously pushed the demand of spindles with higher speed and higher reliability. In order to design, analyze, and test spindles in a virtual environment, accurate modeling of the spindle dynamics during the running state is essential. This paper investigates the variations of interference fit and bearing preload condition induced by centrifugal expansion deformations at high speed. Firstly, the elastic expansion deformations of the rotating parts due to centrifugal force are calculated based on mechanics of elasticity. It is found that the centrifugal expansion deformation of the bearing inner ring is much larger than the deformation of the shaft when the rotational speed increases, and therefore the amount of the interference between the shaft and the bearing decreases with the speed. Then, with consideration of the centrifugal expansion deformation, a dynamic model of high-speed rolling ball bearings is presented with experimental validation. With the proposed bearing model, centrifugal effects on the bearing preload condition are studied in detail. It is shown that the bearing contact angle decreases, while the contact load increases with the centrifugal expansion deformation of the bearing inner ring. The radial bearing stiffness increases, whereas the axial bearing stiffness decreases a little, due to the resultant effects of the decreased contact angle and the increased contact load. The preload condition of the spindle bearing is strengthened by the centrifugal expansion effect of the bearing inner ring.

Keywords: high-speed spindle, rolling bearing, centrifugal effect, radial expansion, bearing preload.

1. Introduction

High-speed machining technology is widely used in aerospace, automotive, electronics and many other industries. Trend of the high-speed machining has pushed the continuous demand of higher speed and higher power for machining tools. As the key component of high-speed machine tools, the spindle affects the overall performance of the machine tool. In order to design, analyze, and test spindles in a virtual environment before resorting to costly physical trials, accurate modeling of spindle dynamics is essential [1].

The rotating components of a high-speed spindle contain shaft, bearings, sleeves, etc. The joint state between each part affects the dynamic behavior and rotating accuracy of the spindle system. The angular contact bearing is still most commonly used today in high-speed spindles due to its low cost, high precision and acceptable speed limit. For the assembly of the shaft/bearing system, it is critical that the spindle shaft is always tightly fitted into the bearing bore, and therefore interference fit is applied between the bearing bore and the spindle shaft. When the shaft is pressed into the bearing, the two parts interfere with each others' occupation of space; the result is that they elastically deform slightly, each being compressed and rotating in unison. The amount of interference is determined by rotating speeds, accuracy and rigidity of the spindle system. In practice, engineers choose the interference allowance according to bearing manufacturer's standard, which can satisfy most needs of bearings in the range of low speed. However, at high speed, the dynamic characteristics variation of the high-speed spindle induced by speed effects cannot be ignored any more. One phenomenon is that the shaft and bearing inner ring expand radially due to centrifugal force, which leads to the change of the joint state

between the shaft and the bearing, as shown in Fig. 1. For the bearing, the centrifugal expansion deformations also induce the variation of internal clearance, which will change the bearing preload condition. If the internal clearance of the bearing becomes smaller than the specified value, the breakage of oil film and seizure due to excessive contact stress may lead to the reduction of bearing life, and even spindle vibration and noise.

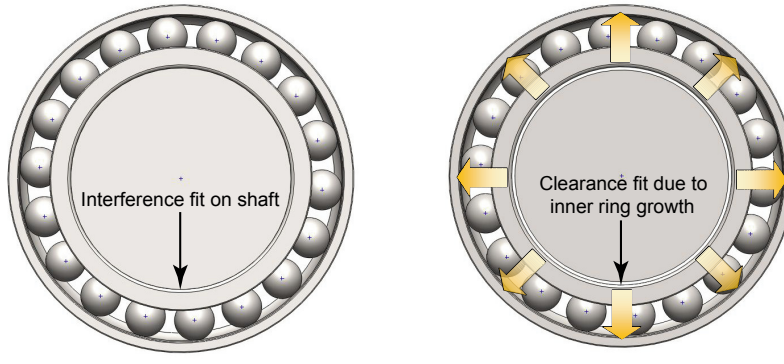

(a) Low speed (b) High speed

Fig. 1. The change of connected state between the shaft and the bearing

Considerable studies on the dynamic modeling of machine tool spindles have been carried out [2-8], and comprehensive models of integrated mechanical and thermal characteristics have been developed to predict the spindle dynamics at high speed. Since the bearing preload has a great affect on the static and dynamic properties of high-speed spindles, many works related to the preload issues have been carried out, which include bearing preload monitoring [9, 10], control [11, 12], and optimization [13]. However, few studies have been performed on the variation of interference fit and bearing preload condition induced by the centrifugal force. Wang et al. [14] studied the effect of the interference fit and axial preload of high-speed angular contact ball bearings, but the variation of the interference fit due to centrifugal force is not considered. Kim et al. [15] investigated the shrink fits and internal clearance variation for ball bearing of machine tool. They presented a finite element model to examine the influences of thermal expansion and centrifugal force on the bearing preload, fitting and clearance variation. However, the influences of the clearance variation on the bearing dynamics were not given. Cao et al. [16] studied the dynamics of high speed spindles with respect to constant and rigid bearing preload mechanisms, but the elastic expansion deformations of rotating parts due to the centrifugal force are not included.

This paper is concerned with the variation of interference fit and the preload condition of bearings in a high-speed spindle system. Elastic expansion deformations of the rotating parts due to the centrifugal force are calculated and the variation of interference fit between the shaft and the bearing at high speed is analyzed. With consideration of the centrifugal expansion deformations, a dynamic model for high-speed bearings is presented with experimental validation. The centrifugal effects on the bearing preload condition are studied to reveal the rule of how the dynamic properties of spindle bearings change with the rotational speed.

The rest of the paper is organized as follows. In Section 2, the elastic expansion deformations of rotating parts due to centrifugal force are calculated and the interference fit of the spindle shaft and the bearing are analyzed. Modeling of high-speed rolling ball bearings is presented in Section 3, while the experimental validation is given in Section 4. In Section 5, the centrifugal effects on the bearing preload condition are studied in detail. Finally, the conclusions are given in Section 6.

2. Elastic expansion deformations of rotating parts due to centrifugal force

In this Section, the elastic expansion deformations of rotating parts due to the centrifugal force are calculated based on mechanics of elasticity. A plane strain problem is assumed for calculating the radial elastic deformation of the shaft, while a plane stress problem is assumed for the bearing inner ring. Both calculations are carried out in the cylindrical co-ordinate system. The variation of the interference fit between the spindle shaft and the bearing is analyzed as well.

2. 1. Elastic expansion deformation of the spindle shaft

Consider a shaft with inner radius *a* and outer radius *b*, as shown in Fig. 2. The shaft rotates with a constant rotational speed ω. The shaft is axisymmetric with a length much larger than its diameter. Shaft rotation produces a centrifugal force that creates an internal stress and elastic expansion deformation in the radial direction. Because of the Poisson effect, normal stresses in one direction produce normal strain in the lateral direction. The radial stress in the rotating shaft creates axial stress in the shaft. Since the boundary condition is free in axial direction, the length of the shaft will be shortened due to the Poisson effect.

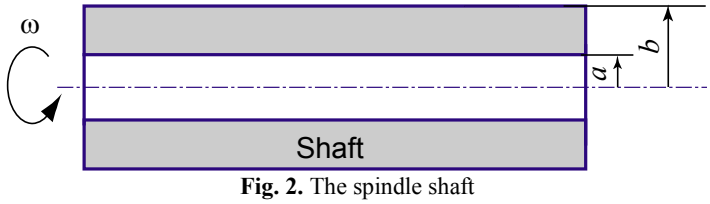

Fig. 2. The spindle shaft

For calculating the radial elastic deformation of the shaft due to centrifugal force, a plane strain problem is assumed and the cylindrical co-ordinate system is used. Due to D'Alembert's principle, the shaft can be considered stationary and the inertia force of a unit volume originating from centrifugal acceleration is expressed as:

$$f_r = \rho\omega^2 r \tag{1}$$

where ρ is the shaft density, ω is the rotating speed and r is the radius vector. In this case the equilibrium equation for the shaft in radial direction is given as follows:

$$\frac{\mathrm{d}\sigma_r}{\mathrm{d}r} + \frac{\sigma_r - \sigma_\theta}{r} + \rho\omega^2 r = 0\,, \tag{2}$$

where σ_r and σ_θ are the radial and the circumferential stress. According to Hooke's Law, the following equation is obtained:

$$\left.\begin{aligned} \varepsilon_r &= \frac{1-\nu^2}{E}\left(\sigma_r - \frac{\nu}{1-\nu}\sigma_\theta\right) \\ \varepsilon_\theta &= \frac{1-\nu^2}{E}\left(\sigma_\theta - \frac{\nu}{1-\nu}\sigma_r\right) \end{aligned}\right\}, \tag{3}$$

where ε_r and ε_θ are the strain variables in the radial and circumferential directions, E and ν are Young's modulus and Poisson's ratio which are the same in the radial and the circumferential directions for isotropic materials. In accordance with axisymmetry and plain strain assumption, the strain-displacement relations can be written as:

$$\varepsilon_r = \frac{\mathrm{d}u_r}{\mathrm{d}r}, \quad \varepsilon_\theta = \frac{u_r}{r}, \tag{4}$$

where u_r is the elastic expansion deformation in the radial direction of the shaft due to the centrifugal force. The compatibility equation for the plane strain is given as:

$$\sigma_\theta - \sigma_r = (1-\nu) r \frac{\mathrm{d}\sigma_\theta}{\mathrm{d}r} - \nu r \frac{\mathrm{d}\sigma_r}{\mathrm{d}r}. \tag{5}$$

Combining Eq. (3) and Eq. (4), the elastic expansion deformation u_s of the shaft due to the centrifugal force is expressed as:

$$u_s = u_r = \frac{r(1-\nu^2)}{E}\left(\sigma_\theta - \frac{\nu}{1-\nu}\sigma_r\right). \tag{6}$$

There are two boundary conditions at the inner surface ($r = a$) and the outer surface ($r = b$) of the shaft. The inner surface is free where the radial stress is zero. The outer surface of the shaft is pressed into the bearing inner ring, and therefore the stress of the pressed part is assumed as P. The boundary conditions are expressed as:

$$\sigma_r\big|_{r=a} = 0, \qquad \sigma_r\big|_{r=b} = P. \tag{7}$$

Applying these boundary conditions to solve σ_r and σ_θ, we can express u_s in an explicit form:

$$u_s(r) = \frac{(1+\nu)(3-2\nu)}{8E(1-\nu)}\rho\omega^2 r\left((1-2\nu)(a^2+b^2) + \frac{a^2b^2}{r^2} - \frac{1-2\nu}{3-2\nu}r^2\right) + \frac{1+\nu}{E}\frac{Pb^2}{b^2-a^2}\left(1-2\nu+\frac{a^2}{r^2}\right). \tag{8}$$

2. 2. The elastic expansion deformation of the bearing inner ring

Consider a rolling ball bearing whose inner ring rotates with a constant rotational speed ω, as shown in Fig. 3. The inner radius and the outer radius of the bearing inner ring are denoted as b and c. The stress generated by the press fitting is assumed as P.

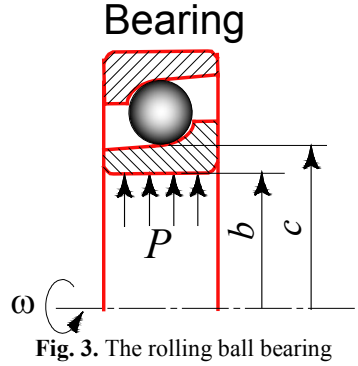

Fig. 3. The rolling ball bearing

To calculate the radial elastic deformation of the bearing inner ring, a plane stress problem is assumed and the cylindrical co-ordinate system is used as well. The following solving process is similar to the shaft problem as presented in Section 2.1.

Due to D'Alembert's principle, the inertia force of a unit volume originating from centrifugal acceleration is expressed as $f_r = \rho\omega^2 r$. The equilibrium equation for the bearing inner ring in radial direction is given as:

$$\frac{\mathrm{d}\sigma_r}{\mathrm{d}r}+\frac{\sigma_r-\sigma_\theta}{r}+\rho\omega^2 r=0\,. \tag{9}$$

According to Hooke's Law, the following equations are obtained:

$$\left.\begin{aligned}\varepsilon_r&=\frac{1}{E}\left(\sigma_r-\nu\sigma_\theta\right)\\ \varepsilon_\theta&=\frac{1}{E}\left(\sigma_\theta-\nu\sigma_r\right)\end{aligned}\right\}. \tag{10}$$

In accordance with the axisymmetry and plain stress assumption, the strain-displacement relations can be written as:

$$\varepsilon_r=\frac{\mathrm{d}u_r}{\mathrm{d}r},\quad \varepsilon_\theta=\frac{u_r}{r}, \tag{11}$$

The compatibility equation for plane stress is given as:

$$\varepsilon_\theta-\varepsilon_r+r\frac{\mathrm{d}\varepsilon_\theta}{\mathrm{d}r}=0\,. \tag{12}$$

Combining Eq. (10) and Eq. (11), the elastic expansion deformation u_b of the bearing inner ring due to centrifugal force is expressed as:

$$u_b=u_r=\frac{r}{E}\left(\sigma_\theta-\nu\sigma_r\right). \tag{13}$$

There are two boundary conditions at the inner surface ($r=b$) and the outer surface ($r=c$) of the bearing inner ring. The outer surface is free where the radial stress is zero. The inner surface of the bearing inner ring is tightly fitted with the stress *P*. The boundary conditions are expressed as:

$$\sigma_r\big|_{r=b}=P,\qquad \sigma_r\big|_{r=c}=0\,. \tag{14}$$

σ_r and σ_θ are calculated by applying these boundary conditions, and then u_b can be expressed explicitly:

$$\begin{aligned}u_b\left(r\right)=&\frac{3+\nu}{8E}\rho\omega^2 r\left(\left(1-\nu\right)\left(b^2+c^2\right)+\left(1+\nu\right)\frac{b^2c^2}{r^2}-\frac{1-\nu^2}{3+\nu}r^2\right)+\\ &\frac{Pb^2r}{\left(b^2-c^2\right)E}\left(1-\nu+\frac{c^2}{r^2}\left(\nu+1\right)\right)\end{aligned}. \tag{15}$$

2. 3. The variation of the interference fit between the spindle shaft and the bearing

Fig. 4 shows the assembly of a shaft-bearing system. To ensure the reliability, the contact pressure between the shaft and the bearing bore should be larger than zero after the press fitting. The centrifugal expansion deformations of the shaft and the bearing inner ring at the contact surface ($r=b$) can be denoted as $u_s\left(b\right)$ and $u_b\left(b\right)$, which can be calculated by Eq. (8) and Eq. (15), respectively.

The radial elastic expansions of the shaft and the bearing inner ring due to the centrifugal force are provided in Fig. 5, in which case *a* = 16 mm, *b* = 35 mm and *c* = 40 mm. As the speed increases, the centrifugal expansion deformation of the bearing inner ring is much faster than the deformation of the shaft. Therefore, the centrifugal expansion deformation of the shaft doesn't change the internal clearance of the bearing. However, the amount of the interference between the shaft and the bearing decreases with the rotational speed. When the speed increases to the limited speed, the amount of the interference becomes zero and the interference fit fails.

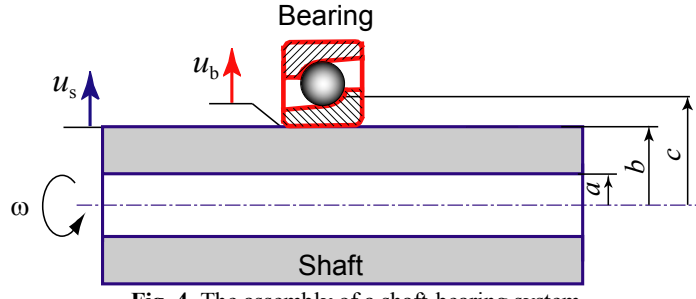

Fig. 4. The assembly of a shaft-bearing system

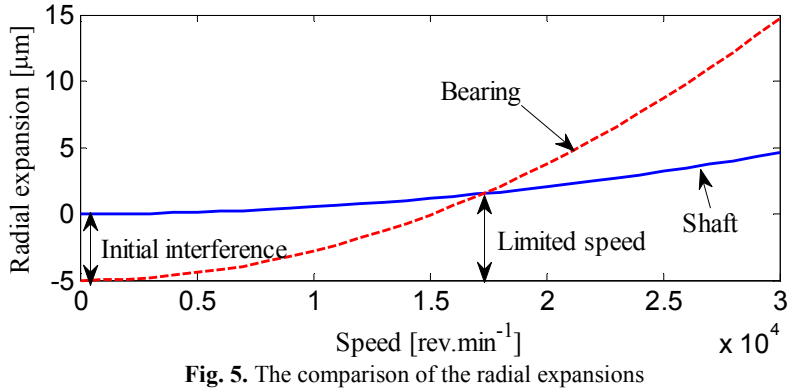

Fig. 5. The comparison of the radial expansions

3. Modeling of high-speed rolling ball bearings

Bearings play an important role in the high-speed spindle system. The purpose of modeling the bearing is to calculate the bearing stiffness accurately, which has the greatest affect on the static and dynamic properties of the spindle systems. Jones [17] developed a general theory for the load-deflection analysis of angular contact ball bearings under high-speed operation. However, the thermal effect and the centrifugal-induced elastic deformation were not considered. In this study, the elastic expansion deformations of the spindle shaft and the bearing inner ring due to the centrifugal force are added to update the Jones' bearing model. The thermal deformations, which are computed separately by a specialized model of heat transfer and thermal deformations [7], are also included.

Under the working condition, the bearing rotates at high speeds with applied axial loads and/or radial loads. Consequently, the relative positions between the inner ring, ball and outer ring change. Based on the Jones' bearing model, the geometry relations of the bearings in the *X-Y* plane are shown in Fig. 6.

The bearing is modeled as 'bearing element'. Each 'bearing element' consists of two nodes-the inner ring node and the outer ring node. The motion vectors of bearing nodes are expressed by $\boldsymbol{q}_i$ (the inner ring node) and $\boldsymbol{q}_o$ (the outer ring node), respectively:

$$\boldsymbol{q}_i = \left\{\delta_{xi}, \delta_{yi}, \delta_{zi}, \gamma_{yi}, \gamma_{zi}\right\}^T, \ \boldsymbol{q}_o = \left\{\delta_{xo}, \delta_{yo}, \delta_{zo}, \gamma_{yo}, \gamma_{zo}\right\}^T. \tag{16}$$

Assume that the outer ring node is fixed to the housing, the relative displacement between the inner ring and the outer ring is:

$$\Delta\boldsymbol{q} = \left\{\Delta\delta_x, \Delta\delta_y, \Delta\delta_z, \Delta\gamma_y, \Delta\gamma_z\right\}^T, \tag{17}$$

where $\Delta\delta_x = \delta_{xi} - \delta_{xi}$, $\Delta\delta_y = \delta_{yi} - \delta_{yo}$, $\Delta\delta_z = \delta_{zi} - \delta_{zo}$, $\Delta\gamma_y = \gamma_{yi} - \gamma_{yo}$, $\Delta\gamma_z = \gamma_{zi} - \gamma_{zo}$.

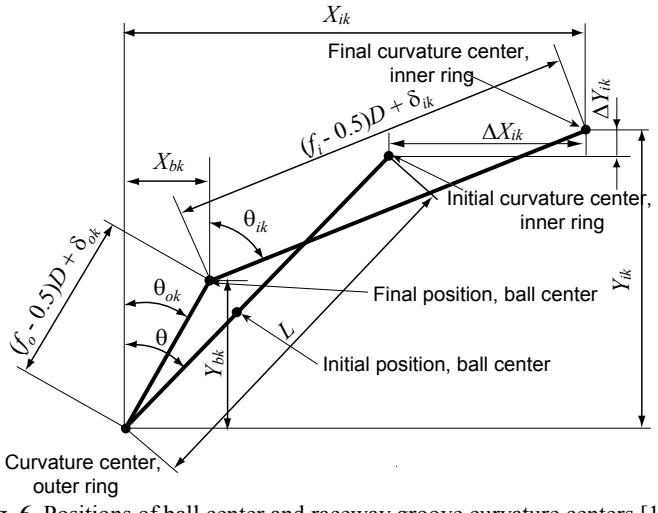

Fig. 6. Positions of ball center and raceway groove curvature centers [18]

Due to external loads, the inner ring and the ball move to a new position. The change of the inner ring's curvature center is expressed as:

$$\begin{cases} \Delta X_{ik} = \Delta\delta_x - \Delta\gamma_z r_{ic}\cos\varphi_k + \Delta\gamma_y r_{ic}\sin\varphi_k \\ \Delta Y_{ik} = \Delta\delta_y\cos\varphi_k + \Delta\delta_z\sin\varphi_k + \varepsilon_{ir} + u_b - \varepsilon_{or} \end{cases}, \tag{18}$$

where $r_{ic} = D_m/2 + (f_i - 0.5)D\cos\theta$, D_m is the pitch diameter and θ is the contact angle, ε_{ir} and ε_{or} are the thermal expansions of the inner ring and the outer ring, which can be obtained by the thermal model discussed in [7], u_b is the centrifugal expansion deformation of the inner ring, which can be calculated by using Eq. (15).

From Fig. 6, the following geometric equations can be obtained using the Pythagorean Theorem:

$$\begin{cases} \left(X_{ik} - X_{bk}\right)^2 + \left(Y_{ik} - Y_{bk}\right)^2 - \left[\left(f_i - 0.5\right)D + \delta_{ik}\right]^2 = 0 \\ {X_{bk}}^2 + {Y_{bk}}^2 - \left[\left(f_o - 0.5\right)D + \delta_{ok}\right]^2 = 0 \end{cases}, \tag{19}$$

where $X_{ik} = L\sin\theta + \Delta X_{ik}$, $Y_{ik} = L\cos\theta + \Delta Y_{ik}$, δ_{ik} is the ball-inner raceway contact deformation and δ_{ok} is the ball-outer raceway contact deformation.

Considering the plane passing through the bearing axis and the center of a ball located at azimuth φ_k, the load diagram obtains in Fig. 7 without consideration of non-coplanar friction forces.

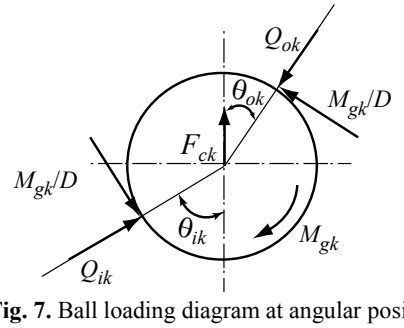

Fig. 7. Ball loading diagram at angular position φ_k

From Fig. 8 the equilibrium of forces in the horizontal and vertical directions are given as:

$$\begin{cases} Q_{ok}\cos\theta_{ok} - \dfrac{M_{gk}}{D}\sin\theta_{ok} - Q_{ik}\cos\theta_{ik} + \dfrac{M_{gk}}{D}\sin\theta_{ik} - F_{ck} = 0 \\ Q_{ok}\sin\theta_{ok} + \dfrac{M_{gk}}{D}\cos\theta_{ok} - Q_{ik}\sin\theta_{ik} - \dfrac{M_{gk}}{D}\cos\theta_{ik} = 0 \end{cases} \tag{20}$$

where the centrifugal force F_{ck} and the gyroscopic moment M_{gk} of the k_{th} ball are taken into account.

Combine Eq. (19) and Eq. (20). The iteration method is used to determine the values of X_{bk}, Y_{bk}, δ_{ik}, δ_{ok}. Then the contact loads in Eq. (20) are calculated by Hertzian theory for spherical contact as:

$$Q_{ik} = K_i\delta_{ik}^{3/2}, \qquad Q_{ok} = K_o\delta_{ok}^{3/2}, \tag{21}$$

where K_i and K_o are the load-deflection coefficients.

The force vector $\boldsymbol{F}_i = \left\{F_{xi}, F_{yi}, F_{zi}, M_{yi}, M_{zi}\right\}^T$ applied on the inner ring of the bearing is given as:

$$\begin{cases} F_{xi} = \sum\limits_{k=1}^{N}\left(Q_{ik}\sin\theta_{ik} + \dfrac{M_{gk}}{D}\cos\theta_{ik}\right) \\ F_{yi} = \sum\limits_{k=1}^{N}\left(Q_{ik}\cos\theta_{ik} - \dfrac{M_{gk}}{D}\sin\theta_{ik}\right)\cos\varphi_k \\ F_{zi} = \sum\limits_{k=1}^{N}\left(Q_{ik}\cos\theta_{ik} - \dfrac{M_{gk}}{D}\sin\theta_{ik}\right)\sin\varphi_k \\ M_{yi} = +\sum\limits_{k=1}^{N}\left\{r_{ic}\left(Q_{ik}\sin\theta_{ik} + \dfrac{M_{gk}}{D}\cos\theta_{ik}\right) - f_i M_{gk}\right\}\sin\varphi_k \\ M_{zi} = -\sum\limits_{k=1}^{N}\left\{r_{ic}\left(Q_{ik}\sin\theta_{ik} + \dfrac{M_{gk}}{D}\cos\theta_{ik}\right) - f_i M_{gk}\right\}\cos\varphi_k \end{cases} \tag{22}$$

Similarly, the force vector $\boldsymbol{F}_o = \left\{F_{xo}, F_{yo}, F_{zo}, M_{yo}, M_{zo}\right\}^T$ applied on the outer ring of the bearing can be obtained. By finding the derivatives of forces with respect to displacements, the stiffness matrix of the bearing can be obtained as:

$$\boldsymbol{K}_B = \frac{\partial \boldsymbol{F}_i}{\partial \boldsymbol{q}_i} = \frac{\partial \boldsymbol{F}_o}{\partial \boldsymbol{q}_o}. \tag{23}$$

4. Experimental validations

The shaft-bearing-housing model is validated by using a test high-speed spindle in the University of British Columbia. The test spindle consists of shaft, angular contact ball bearings, housing, drawbar, bearing and other accessories, as shown in Fig. 8. The spindle has two front bearings GMN-HYKH61914 and three rear bearings GMN-HYKH61911 in an O-type configuration. The eddy current sensors (Lion Precision 034092, resolution: 0.1 μm) are embedded in the spindle to measure the radial displacement of the shaft.

Displacement measurement due to the radial expansion. During the test process, the eddy current sensor in the middle of the shaft was chosen, where the inner diameter and the outer diameter of the shaft is 28 mm and 67 mm, respectively. The spindle speed was increased from 0

to 12.000 rev/min with an increment of 2.000 rev/min. The displacement due to the radial expansion was measured at each speed. The tests were repeated five times and the average values are used. The comparison of the simulated and the measured expansion displacements are displayed in Fig. 9. Although the radial expansion is very slight, the agreement between the simulation and the measurement is acceptable.

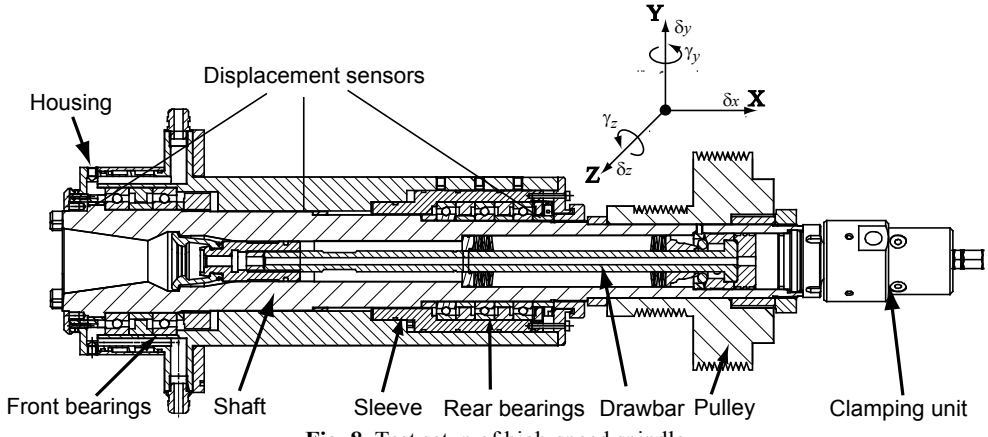

Fig. 8. Test setup of high-speed spindle

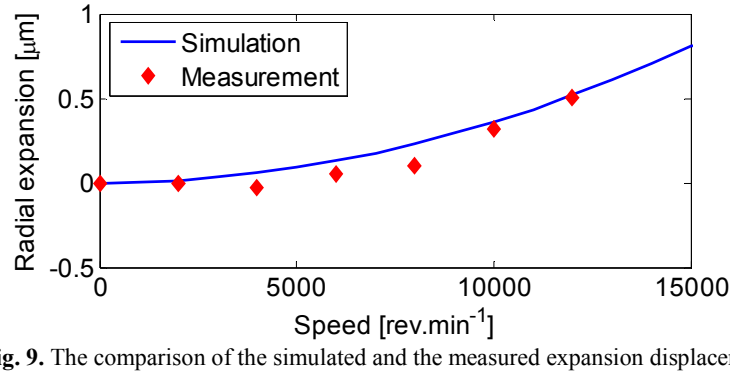

Fig. 9. The comparison of the simulated and the measured expansion displacements

Dynamic tests of the spindle during the running state. In Section 3, the elastic expansion deformations of the spindle shaft and the bearing inner ring induced by centrifugal forces are included to update the Jones' bearing model. Since the bearing stiffness is not easy to measure when the spindle is rotating at high speeds, alternatively, the frequency response function (FRF) of the spindle-bearing system can be used as a criterion to validate the bearing model. If the natural frequencies from the simulation match those from experiments, the dynamic stiffness of bearings should be correct because the shaft, housing, pulley and other accessories can be reasonably modeled using finite element method [16, 19].

The test spindle was installed on a machine tool to study its dynamics during rotation. The experimental setup is shown in Fig. 10.

A dummy tool without any flutes was used, and the FRF at the tool tip was measured using a laser vibrometer and a modal hammer. The measurements were conducted by CutPro-MalTF® Fourier Analyzer under various spindle speeds.

The comparison of the simulated and the experimental FRFs at the tool tip in the *X*-direction is displayed in Fig. 11, in which the spindle speed is 12.000 rev/min. The dominant mode is mainly determined by the bearing stiffness. Despite the disturbance of the rotating frequency and

its harmonics in the measured FRF, the simulations and experiments are still in a good agreement, especially around the dominant mode. Therefore, the accuracy of the high-speed bearing model is verified at high speed.

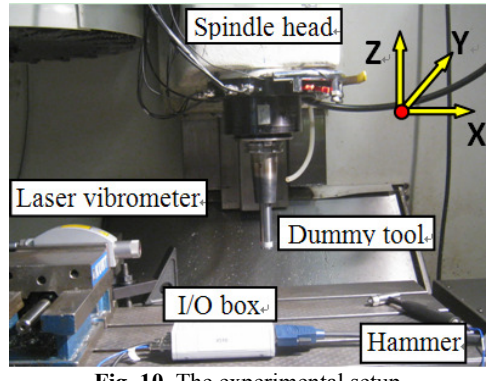

Fig. 10. The experimental setup

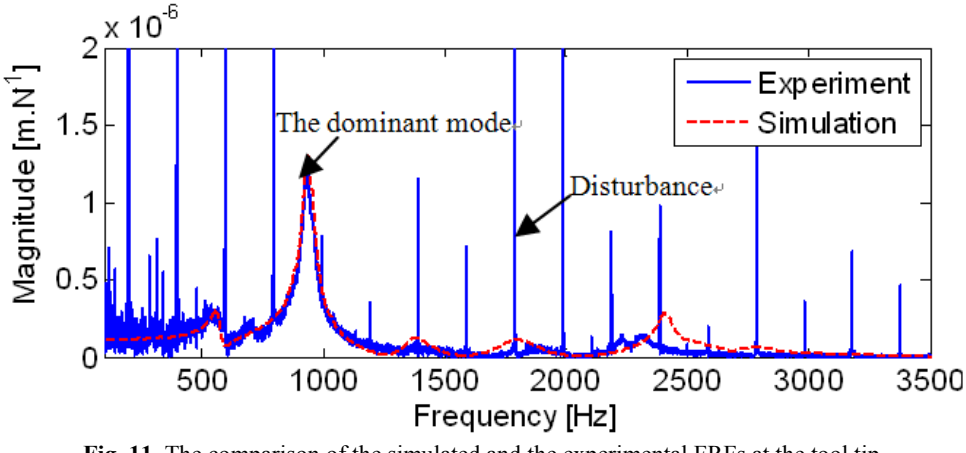

Fig. 11. The comparison of the simulated and the experimental FRFs at the tool tip

5. The centrifugal effects on the bearing preload condition

Bearing preload can be regarded as negative internal clearance in the bearing. Proper preload of angular contact bearings is desirable for improving the rigidity, rotating accuracy, and bearing life of spindles. However, due to the centrifugal and thermal effects, the bearing preload condition in the high-speed spindle is not constant. On the one hand, the increased preload will lead to inappropriate negative clearance, which can cause excessive rolling contact stresses and eventually result in bearing seizure. On the other hand, the decreased preload may lower the system rigidity and the rotating accuracy.

Based on the presented high-speed bearing model, the centrifugal effects at high speed on the bearing preload condition are focused in this study. The changes of bearing dynamic characteristics with the rotating speed are investigated to estimate the bearing preload condition. The bearing HYKH61914 is used as an example. The centrifugal expansion deformation of the outer surface of the bearing inner ring is calculated by using Eq. (15). The relationship between the centrifugal expansion and the rotating speed is shown in Fig. 12. When the speed reaches 15.000 rev/min, the centrifugal expansion deformation of the bearing inner ring is 4.9 μm.

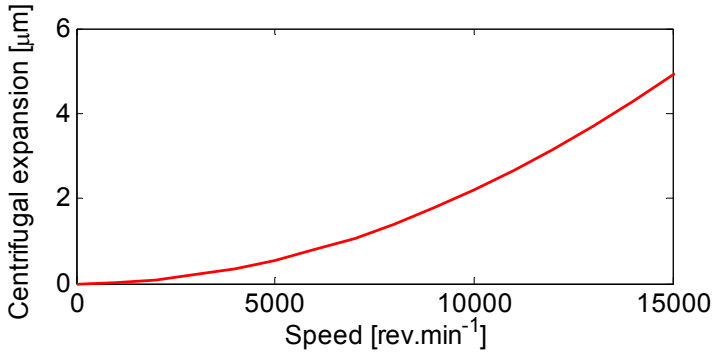

Fig. 12. The centrifugal expansion of the bearing inner ring (HYKH61914)

The changes of contact angle and contact load with the radial expansion of the bearing inner ring are shown in Fig. 13. It can be seen that, as the radial expansion deformation of the bearing inner ring increases, the contact angle decreases (Fig. 13a), whereas the contact load increases (Fig. 13b).

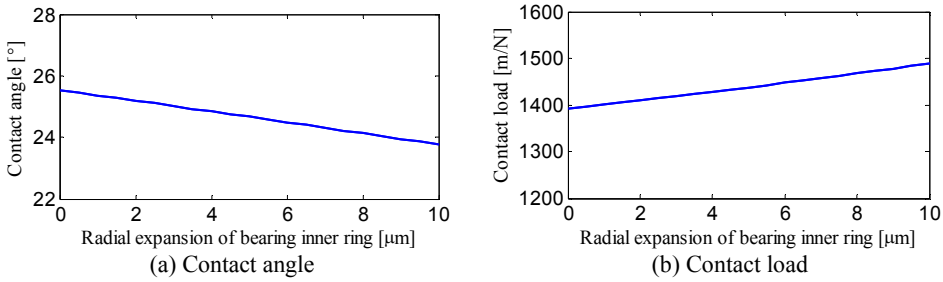

(a) Contact angle (b) Contact load

Fig. 13. Changes of contact angle and contact load with the radial expansion of the bearing inner ring

The changes of bearing stiffness with the radial expansion of the bearing inner ring are shown in Fig. 14. With the increased radial expansion of the bearing inner ring, the radial stiffness of the bearing increases, whereas the axial stiffness decreases a little due to resultant effect of the decreased contact angle and the increased contact load.

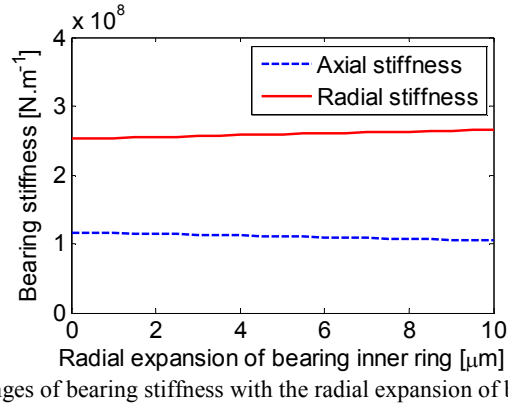

Fig. 14. Changes of bearing stiffness with the radial expansion of bearing inner ring

With consideration of the centrifugal force, gyroscopic moment of balls and the radial expansion of the bearing inner ring, the bearing characteristics (i.e., contact angles, contact loads

and bearing stiffness) are calculated with the extended Jones' bearing model. To study the effects of the centrifugal expansion deformation, two cases are considered, i.e., with and without the centrifugal expansion of the bearing inner ring.

The outer contact angle and the inner contact angle change with the rotational speed, as shown in Fig. 15. In both cases, the outer contact angle decreases with the speed, while the inner contact angle increases with the speed due to the centrifugal force of the ball. As the contact angle of the bearing decreases with the radial expansion of bearing inner ring, the contact angles (including both the inner contact angle and the outer contact angle) in the case of centrifugal expansion of the bearing inner ring are lower in comparison to the case when there is no centrifugal expansion of the bearing inner ring.

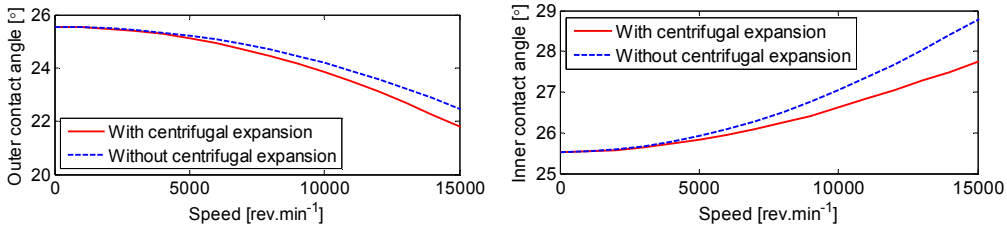

(a) Outer contact angle (b) Inner contact angle

Fig. 15. Changes of contact angles with the rotational speed

Fig. 16 shows the changes of the outer contact load and the inner contact load with the rotational speed. The outer contact load increases with the speed, while the inner contact load decreases with the speed in both cases (with and without centrifugal expansion). As the contact load of the bearing increases with the radial expansion of the bearing inner ring, the contact loads (including both the inner contact load and the outer contact load) in the case of centrifugal expansion of the bearing inner ring are higher than in the case of no centrifugal expansion. In terms of contact load, the bearing preload is increased by the centrifugal expansion of the bearing inner ring at high speed.

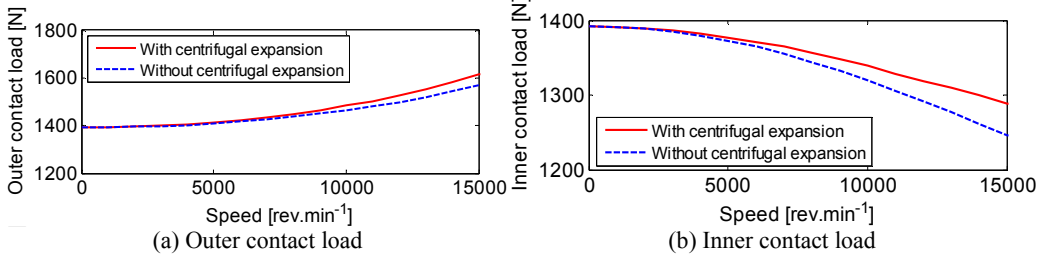

(a) Outer contact load (b) Inner contact load

Fig. 16. Changes of contact loads with the rotational speed

The changes of the bearing stiffness with the rotational speed are displayed in Fig. 17. Due to the reduced contact load and increased contact angle at the ball/inner ring contact interface caused by the centrifugal force of balls, both the axial stiffness and the radial stiffness of the bearing decrease with the speed. Within the speed range of 0 – 15.000 rev/min the effect of centrifugal expansion deformation on the axial stiffness of the bearing can be neglected. When the speed reaches 15.000 rev/min, the radial stiffness is increased by ca. 10 % due to the centrifugal expansion deformation of the bearing inner ring. Since the radial stiffness increases, the preload condition of the bearing is strengthened.

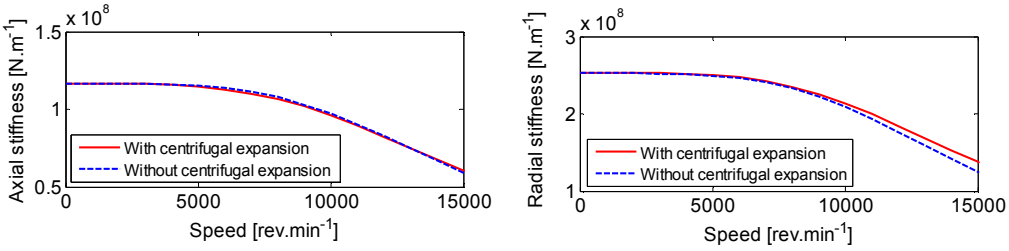

(a) Axial stiffness (b) Radial stiffness

Fig. 17. The changes of bearing stiffness with the rotational speed

6. Conclusions

In this study, the variations of interference fit and bearing preload condition induced by centrifugal expansion deformations at high speed are investigated. The results have demonstrated that:

1) With the increased rotational speed, the bearing inner ring expands much faster than the shaft due to the centrifugal force. The amount of the interference between the shaft and the bearing decreases with the speed. When the speed increases to the limited speed, the amount of the interference becomes zero and the interference fit fails.

2) The bearing contact angle decreases, while the contact load increases with the centrifugal expansion deformation of the bearing inner ring. The radial bearing stiffness increases, whereas the axial bearing stiffness decreases a little due to the resultant effect of the decreased contact angle and the increased contact load. The preload condition of the spindle bearing is strengthened by the centrifugal expansion effect of the bearing inner ring.

Acknowledgments

The authors wish to express their heartfelt gratitude to Professor Yusuf Altintas from Manufacturing Automation Laboratory (MAL), The University of British Columbia, for his valuable instruction, guidance and support throughout this work. All the experiments of this paper were carried out in MAL. This work is jointly supported by National Natural Science Foundation of China (No. 51105294, 51035007), Research Fund for the Doctoral Program of Higher Education of China (No. 20110201120029) and the Fundamental Research Funds for the Central University.

References

[1] **Altintas Y., Cao Y.** Virtual design and optimization of machine tool spindles. CIRP Annals - Manufacturing Technology, Vol. 54, Issue 1, 2005, p. 379-382.

[2] **Jorgensen B. R., Shin Y. C.** Dynamics of spindle-bearing systems at high speeds including cutting load effects. Journal of Manufacturing Science and Engineering - Transactions of the ASME, Vol. 120, Issue 2, 1998, p. 387-394.

[3] **Lin C. W., Tu J. F., Kamman J.** An integrated thermo-mechanical-dynamic model to characterize motorized machine tool spindles during very high speed rotation. International Journal of Machine Tools & Manufacture, Vol. 43, Issue 10, 2003, p. 1035-1050.

[4] **Li H. Q., Shin Y. C.** Integrated dynamic thermo-mechanical modeling of high speed spindles, Part 1: Model development. Journal of Manufacturing Science and Engineering - Transactions of the ASME, Vol. 126, Issue 1, 2004, p. 148-158.

[5] **Cao Y. Z., Altintas Y.** Modeling of spindle-bearing and machine tool systems for virtual simulation of milling operations. International Journal of Machine Tools & Manufacture, Vol. 47, Issue 9, 2007, p. 1342-1350.

[6] **Gagnol V., Bougarrou B. C., Ray P., Barra C.** Stability-based spindle design optimization. Journal of Manufacturing Science and Engineering - Transactions of the ASME, Vol. 129, Issue 2, 2007, p. 407-415.

[7] **Holkup T., Cao H., Kolár P., Altintas Y., Zelený J.** Thermo-mechanical model of spindles. CIRP Annals - Manufacturing Technology, Vol. 59, Issue 1, 2010, p. 365-368.

[8] **Jiang S. Y., Zheng S. F.** A modeling approach for analysis and improvement of spindle-drawbar-bearing assembly dynamics. International Journal of Machine Tools & Manufacture, Vol. 50, Issue 1, 2010, p. 131-142.

[9] **Mannan M. A., Stone B. J.** The use of vibration measurements for quality control of machine tool spindles. International Journal of Advanced Manufacturing Technology, Vol. 14, Issue 12, 1998, p. 889-893.

[10] **Spiewak S. A., Nickel T.** Vibration based preload estimation in machine tool spindles. International Journal of Machine Tools & Manufacture, Vol. 41, Issue 4, 2001, p. 567-588.

[11] **Chen J. S., Chen K. W.** Bearing load analysis and control of a motorized high speed spindle. International Journal of Machine Tools & Manufacture, Vol. 45, Issue 12-13, 2005, p. 1487-1493.

[12] **Hwang Y. K., Lee C. M.** Development of automatic variable preload device for spindle bearing by using centrifugal force. International Journal of Machine Tools & Manufacture, Vol. 49, Issue 10, 2009, p. 781-787.

[13] **Jiang S. Y., Mao H. B.** Investigation of variable optimum preload for a machine tool spindle. International Journal of Machine Tools & Manufacture, Vol. 50, Issue 1, 2010, p. 19-28.

[14] **Wang S. G., Xia Y. M.** Effect of the interference fit and axial preload in the stiffness of the high-speed angular contact ball bearing. Journal of University of Science and Technology of China, Vol. 36, Issue 12, 2006, p. 1314-1320.

[15] **Kim W., Lee C. M., Hwang Y. K.** A study on the shrink fits and internal clearance variation for ball bearing of machine tool using FEM. Proceedings of International Multi-Conference of Engineers and Computer Scientists, March 18-20, 2009, Hong Kong, p. 1-5.

[16] **Cao H. R., Holkup T., Altintas Y.** A comparative study on the dynamics of high speed spindles with respect to different preload mechanisms. International Journal of Advanced Manufacturing Technology, Vol. 57, Issue 9-12, 2011, p. 871-883.

[17] **Jones A. B.** A general theory for elastically constrained ball and radial roller bearings under arbitrary load and speed conditions. Journal of Basic Engineering, Transactions of the ASME, Vol. 82, Issue 2, 1960, p. 309-320.

[18] **Harris T. A.** Rolling Bearing Analysis. John Wiley and Sons, New York, 1991.

[19] **Cao H. R., Li B., He Z. J.** Chatter stability of milling with speed-varying dynamics of spindles. International Journal of Machine Tools & Manufacture, Vol. 52, Issue 1, 2012, p. 50-58.